Marine Geology 488 (2025) 107607

Contents lists available at ScienceDirect

Marine Geology

journal homepage: www.elsevier.com/locate/margo

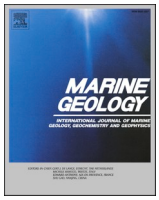

Research Article

^{14}C dating of tsunami deposits in arid environments: How challenging can it be? The example of La Graciosa, Canary Islands

Raphaël Paris [a,*], Franck Lavigne [b,1], Christine Hatté [c,d], Juan Francisco Betancort [e], Jean-Pierre Flandrois [f], Arnauld Vinçon-Laugier [f], Eve Poulallion [f], Simon Falvard [a], Bachtiar W. Mutaqin [g], Christophe Lécuyer [h,a]

[a] Laboratoire Magmas et Volcans, CNRS, IRD, OPGC, Université Clermont Auvergne, Clermont-Ferrand, France
[b] Université Paris 1 Panthéon-Sorbonne, Laboratoire de Géographie Physique, UMR 8591 CNRS, Thiais, France
[c] Laboratoire des Sciences du Climat et de l'Environnement, CNRS, CEA, Université de Versailles Saint-Quentin, Université Paris Saclay, Gif-sur-Yvette, France
[d] Silesian University of Technology, Gliwice, Poland
[e] Departamento de Biología, Universidad de Las Palmas de Gran Canaria, Las Palmas de Gran Canaria, Spain
[f] Laboratoire de Biométrie et Biologie Evolutive, CNRS, Faculté de Médecine Lyon-Sud, Université de Lyon 1, France
[g] Faculty of Geography, Universitas Gadjah Mada, Sekip Utara, Bulaksumur, 55281 Yogyakarta, Indonesia
[h] Laboratoire de Géologie de Lyon, CNRS, Université de Lyon, Villeurbanne, France

ARTICLE INFO

Editor: Shu Gao

Keywords:
Tsunami deposit
Landslide tsunami
Cliff collapse
La Graciosa Island
Canary Islands
Mollusc shells
^{14}C dating
Stable isotopes

ABSTRACT

^{14}C dating of tsunami deposits in arid environments is often challenging, especially when there is no organic material available. The marine bioclasts found in the tsunami deposits thus become the main dating possibility. Apart from the reservoir effect, the main source of uncertainty is the age difference between the shells and the tsunami that transported them. Taking as an example a tsunami deposit on the island of La Graciosa (Canary Islands), we demonstrate that the marine shells (*Patella*) come from different sources, with ^{14}C ages ranging from >45 kBP to 200 BP, the main source being an ancient marine terrace probably of MIS5e age. In addition, we propose a landslide source for this tsunami, the scar of which can be observed on the Famara cliff to the northeast of Lanzarote, just opposite the tsunami deposit outcrops at La Graciosa. In addition to the methodological aspects of shell dating, this study also serves as a reminder that local tsunamis generated by coastal cliff collapses are not a hazard to be neglected.

1. Introduction

The assessment of natural hazards is based on understanding the physical processes specific to each hazard, but it is also necessary to know how to draw lessons from past disasters. When the reference period is short (*e.g.*, catalog of historical events limited to the post-colonial period) and potentially unrepresentative of the different possible scenarios, it is necessary to extend this period by identifying and date even older events, preserved in the geological archives. This approach is therefore partly based on the reliability of the methods used to date these paleo-events.

Our knowledge of the tsunami hazard has progressed considerably thanks to studies of tsunami deposits preserved in coastal sedimentary sequences (Engel et al., 2020). In the vast majority of cases, tsunami deposits are dated indirectly using ^{14}C on *in-situ* soil below or above the tsunami deposit, wood, charcoal, seeds, mosses, bones, shells, artefacts such as pottery, or rip-up clasts of soil sampled inside the tsunami deposit (Kelsey and Witter, 2020; Ishizawa et al., 2020 and references therein). ^{14}C dating of material transported by the tsunami therefore provides a maximum age (*i.e.*, older than the age of the tsunami). Dating tsunami deposits can be challenging in arid coastal environments, where the scarcity of organic material limits the possibilities and forces researchers to turn to other types of materials such as marine bioclasts (bivalve or gastropod shells, coral fragments), which are often present in tsunami deposits. However, several authors reported age differences of several centuries or even several thousand years between shells taken from the same tsunami deposit (*e.g.*, Dominey-Howes et al., 2000; Nichol et al., 2007).

* Corresponding author.
E-mail address: raphael.paris@uca.fr (R. Paris).
[1] Institut Universitaire de France, Paris, France

https://doi.org/10.1016/j.margeo.2025.107607
Received 20 May 2025; Received in revised form 16 June 2025; Accepted 17 June 2025
Available online 24 June 2025

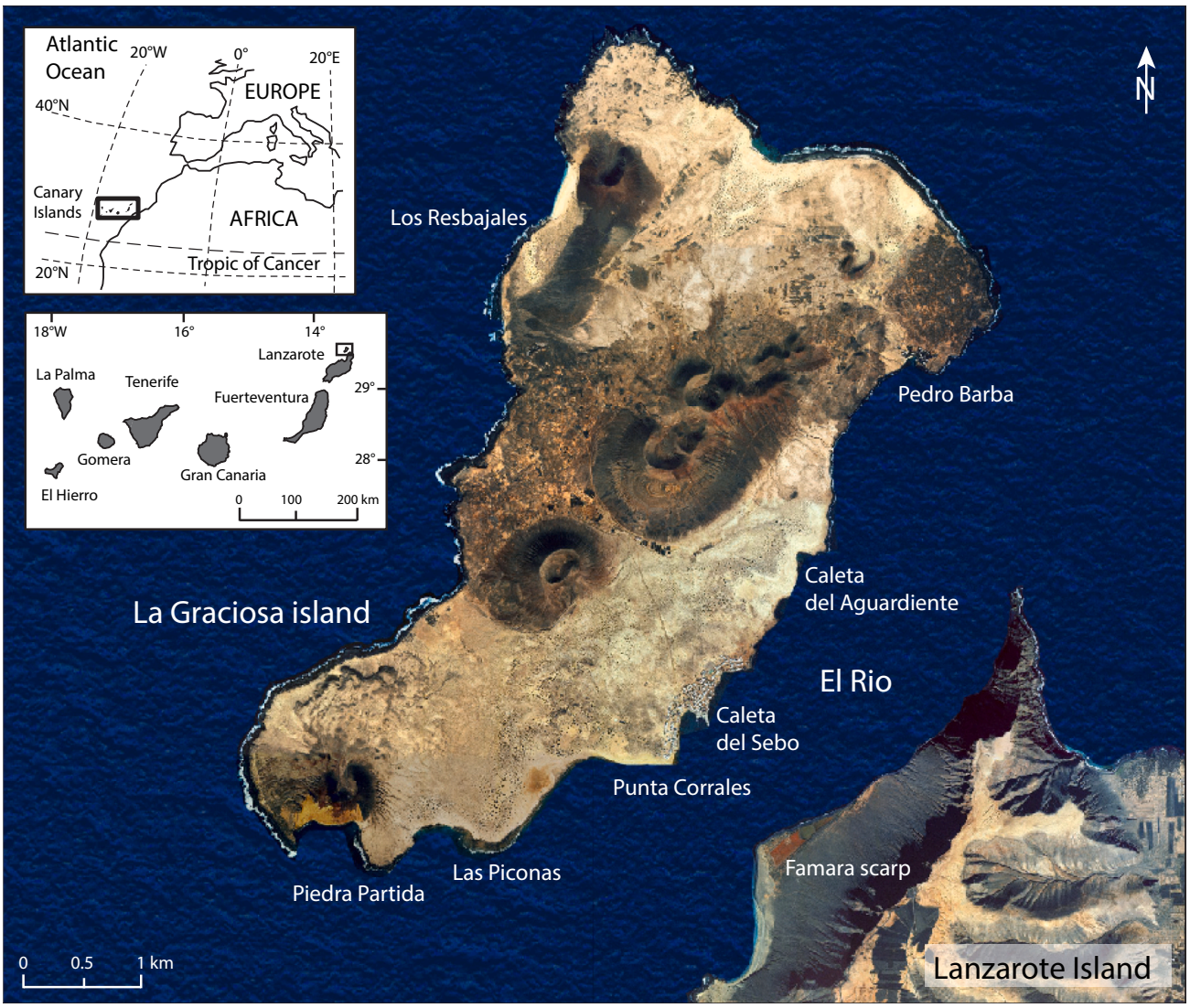

Fig. 1. Location map of La Graciosa Island, Eastern Canary Islands.

^{14}C dating on marine shells also faces the issue of the so-called reservoir age, *i.e.*, the difference between the marine radiocarbon age of a sample that derives its carbon from the marine reservoir and the atmospheric ^{14}C age at the same time. A global marine surface mixed-layer calibration curve, Marine20 (Heaton et al., 2020), is available to provide the mean reservoir age (MRA), but a shift from the global value (ΔR) has to be estimated to fit with the exact location and living period of the sample. Even if some data are available in a database (Reimer and Reimer, 2001), they do not always provide the required temporal resolution and estimating the ΔR constitutes a major challenge in dating the shells of marine molluscs. In some cases, other dating techniques can be applied, such as optically stimulated luminescence (OSL), cosmogenic nuclides, and U/Th (Rixhon et al., 2018; Araoka, 2020; Brill and Tamura, 2020).

In this paper, we explore the advantages and limitations of ^{14}C dating method of mollusc shells preserved in a tsunami deposit on the eastern coast of the island of La Graciosa, in the extreme northeast of the Canary Archipelago. The combination of an arid environment on land and a coastal environment rich in datable shells makes La Graciosa an ideal case study. We also provide evidence that this tsunami was caused by a landslide on the Famara cliff on the neighbouring island of Lanzarote.

2. Study area

The Canary Islands are located in the Eastern Atlantic Ocean (Fig. 1), about 150 km off the west coast of Africa, at a subtropical latitude roughly comprised between 27°N and 29°N for longitudes extending from 18°W to 13°W of Greenwich. The Canary Archipelago belongs to the Macaronesian province, including the Azores, Madeira, Selvagems, and Cabo Verde, which, in addition to their volcanic origins, share biogeographical affinities (Castro et al., 2022). Canary volcanism is the result of a hot spot beneath the African plate (Watts, 1994; Carracedo et al., 1998; Geldmacher et al., 2005). The relative slowness of the plate's movement (2 cm/year towards the northeast) extends the duration of volcanism on each island, leading to several cycles of rejuvenated volcanism, beyond the initial shield building stage. Thus, the eastern islands of Fuerteventura and Lanzarote were mainly formed in the Miocene, but they also experienced eruptions in the Quaternary, and even historical eruptions (Coello et al., 1992; Perez-Torrado et al., 2023).

The island of La Graciosa, with an area of 27 km^2, is located to the north of the island of Lanzarote (Fig. 1). The two islands are separated by *El Rio*, a strait 1–2 km wide and 10–15 m deep. La Graciosa was built on a shallow Quaternary marine platform where volcanic cones erupted lava flows during the Upper Pleistocene and Holocene (Coello et al.,

Fig. 2. Tsunami conglomerate on aeolian deposits at Punta Corrales. A: general view of the outcrop, with the tsunami deposit in discontinuity over Upper Pleistocene aeolian deposits; B: cross-sectional view showing abundant marine shells; C: closer view to tsunami deposit illustrating the bioclastic nature of the sandy matrix.

1992). The maximum altitude of these cones does not exceed 270 m a.s.l. A large surface of the island (> 50 %) is covered by aeolian sands mainly made of marine and continental carbonates, along with minor amounts of clay minerals (Damnati et al., 1996; Menéndez et al., 2014), quartz grains coming from the Sahara (Williamson et al., 2004), and local basaltic clasts (Yanes et al., 2011). These aeolian sands correspond to bioclastic dunes that were formed during glacial-arid periods, when sea level was lower (Petit-Maire et al., 1986; Rognon and Coudé-Gaussen, 1996; Meco et al., 1997). The aeolian deposits are interbedded with paleosols formed during interglacial-humid periods (Yanes et al., 2011). The coasts of the island are mainly made up of cliffs and rocky platforms carved out of volcanic cones and lava flows. The coves are lined with by

Table 1
Pairs of ^{14}C dating from the literature for the Canary Islands. ^{14}C dating of marine and of associated terrestrial components are shown. The reservoir age, R, the deviation towards the global marine calibration (Marine20), and ΔR_{20} are calculated for all individual pair as the weighted average ΔR_{20} from all the pairs.

	Marine component					Terrestrial component				Reservoir age		Deviation / Marine20	
	species	^{14}C age	±			type	species	^{14}C age	±	R [^{14}C yr]	±	$\Delta R_{20\ (68\%)}$	±
Martins et al., 2012													
Tenerife	*Patella sp.*	1260	60			bone	"animal"	950	50	310	80	−215	80
(Canary Islands)	*Patella sp.*	1310	35			bone	"animal"	890	30	420	50	−110	62
	Patella sp.	890	35	930	25	bone	"animal"	520	35	460	50	−186	40
	Patella sp.	980	40										
	Patella sp.	640	60			charred wood		200	80	440	100	−142	124
	Patella sp.	370	40	385	30	charred wood		140	50	260	65	–	
	Patella sp.	400	40										
Fuerteventura	*Patella sp.*	1170	35	1125	25	bone	"animal"	520	35	570	45	5	60
(Canary Islands)	*Patella sp.*	1090	30										
	Patella sp.	1020	35	995	25	bone	"animal"	400	40	570	50	−32	55
	Patella sp.	970	35										
	Patella sp.	1050	35	1095	25	bone	"animal"	460	40	680	50	17	40
	Patella sp.	1140	35										
Soares et al., 2011													
Sao Vicente Island													
(Cape Verde)	*Patella spp.*	860	40			bone	*Capra hircus*	275	60	585	70	−45	86
	Patella spp.	570	35			bone	*Capra hircus*	130	40	440	50	–	
								average ± SD				**−78**	**88**

pebble beaches, whereas the larger bays feature sandy beaches and aeolian deposits.

La Graciosa island is characterized by a "hot desert climate" (BWh) according to the Köppen-Geiger climate classification (Peel et al., 2007). The scarce vegetation consists of halophytic, psammophytic, and xeric scrub species that grow seasonally in response to occasional torrential rains that cumulate to a mean annual precipitation (MAP) of 116 mm (Santana Cordero et al., 2016). The mean annual air temperature (MAAT) is close to 20 °C, with a seasonal range of 6 °C. The trade winds, which carry dust from the Sahara, blow at an average speed of 18.3 km/h (Santana Cordero et al., 2016). Tide range at the Caleta del Sebo harbor is around 1 m.

Since at least the 14th century, and possibly as far back as Roman times, La Graciosa was often the first anchor point for ships coming from Europe (González Viera et al., 1996). The island probably served as a base camp for the first expeditions to make contact with the indigenous people of Lanzarote. However, the island stayed inhabited until the late 19th century, although the inhabitants of Lanzarote used it as pastureland as early as the 16th century (Ayuntamiento de Teguise, 1871; González Viera et al., 1996; Santana Cordero et al., 2016).

In their review of historical tsunamis in the Canary Islands, Galindo et al. (2021) documented a possible tsunami deposit dated 1730 ± 30 BP on the eastern coast of La Graciosa (Fig. 2). The source of this tsunami is unclear. Galindo et al. (2021) evoke distant earthquakes off the coast of Portugal. The purely tectonic earthquakes recorded in the Canary Islands are far too weak in magnitude to generate tsunamis. On the other hand, massive collapses of the flanks of the islands caused mega-tsunamis with wave runups >100 m (Paris et al., 2018 and references therein). These events of exceptional intensity are extremely rare (<10 events during the last million years), but smaller cliff collapses can also occur, generating local tsunamis, as happened on La Gomera Island on November 14, 2020 (Galindo et al., 2021).

3. Methods

3.1. Mapping and characterization of the tsunami deposits

Using the conglomerate interpreted as a tsunami deposit by Galindo et al. (2021) as a reference, we surveyed the entire coast of the island of La Graciosa, with a particular focus on the eastern coast from Piedra Partida to Pedro Barba (Fig. 1). We mapped with GPS all the sedimentological and morphological features potentially linked to a tsunami, such as erosion chevrons, conglomerate deposits, and pebbles and marine shells scattered on the dunes at a height well above that of the storm debris lines. We collected 5 samples of tsunami conglomerate, 1 sample of a marine conglomerate that forms a marine terrace at 0–0.2 m a.s.l. (García-Talavera, 2002), as well as 18 shell samples found in the tsunami conglomerates and other depositional environments such as aeolian deposits, the marine terrace at +0.2 m a.s.l., and present-day beaches. The cementation of the conglomerates made it possible to produce thin sections on small blocks.

X-ray computed tomography (X-CT) was performed on two conglomerate samples using an EasyTom RX-Solutions CT system at the Laboratoire Magmas & Volcans (Clermont-Ferrand, France). The optimum tomography settings were determined at a tube voltage of 90 kV and a current of 195 μA. A 1 mm-thick Al-filter was placed at the exit of the X-ray tube in order to reduce beam hardening. The 1120 tomographic projections were reconstructed with a filtered back-projection algorithm, resulting in tomograms with a pixel resolution of 20 μm, which is sufficient to distinguish most individual grains (clasts) from the matrix and each other. With the aim of studying the sedimentary fabric of a tsunami deposit, we applied the image segmentation workflow proposed by Mitra et al. (2024) to separate the grains from each other in complex sedimentary assemblages such as tsunami deposits. The direction cosines of the three axes of the grains best-fit ellipsoids were then calculated using Blob3D (Ketcham, 2005) to obtain their azimuthal orientation and dip angles. The dataset was filtered to keep only grains larger than 1 mm^3, with smaller grains not being sufficiently resolved.

3.2. ^{14}C dating of mollusc shells

The relatively arid climate of La Graciosa and its poor lithological variety limit dating possibilities. The absence of autigenic quartz and feldspar in the sedimentary formations rules out OSL dating (Brill and Tamura, 2020). Cosmogenic dating can only be applied to coarse clasts with a high concentration of stable chlorine, such as coral boulders (Rixhon et al., 2018). The limited development of soils and vegetation also limits the possibilities of ^{14}C dating, making marine shells the best candidates.

Mollusc shells were first mechanically abraded to remove surface carbonate that can be contaminated by carbonate dissolution, recrystallization, and deposits occurring posteriorly to the death of the animal. For all but the *Patella* C14 12, an aliquot of *ca.* 15 mg of carbonate taken from the outer edges, underwent chemical leaching with HNO_3 0.1 N,

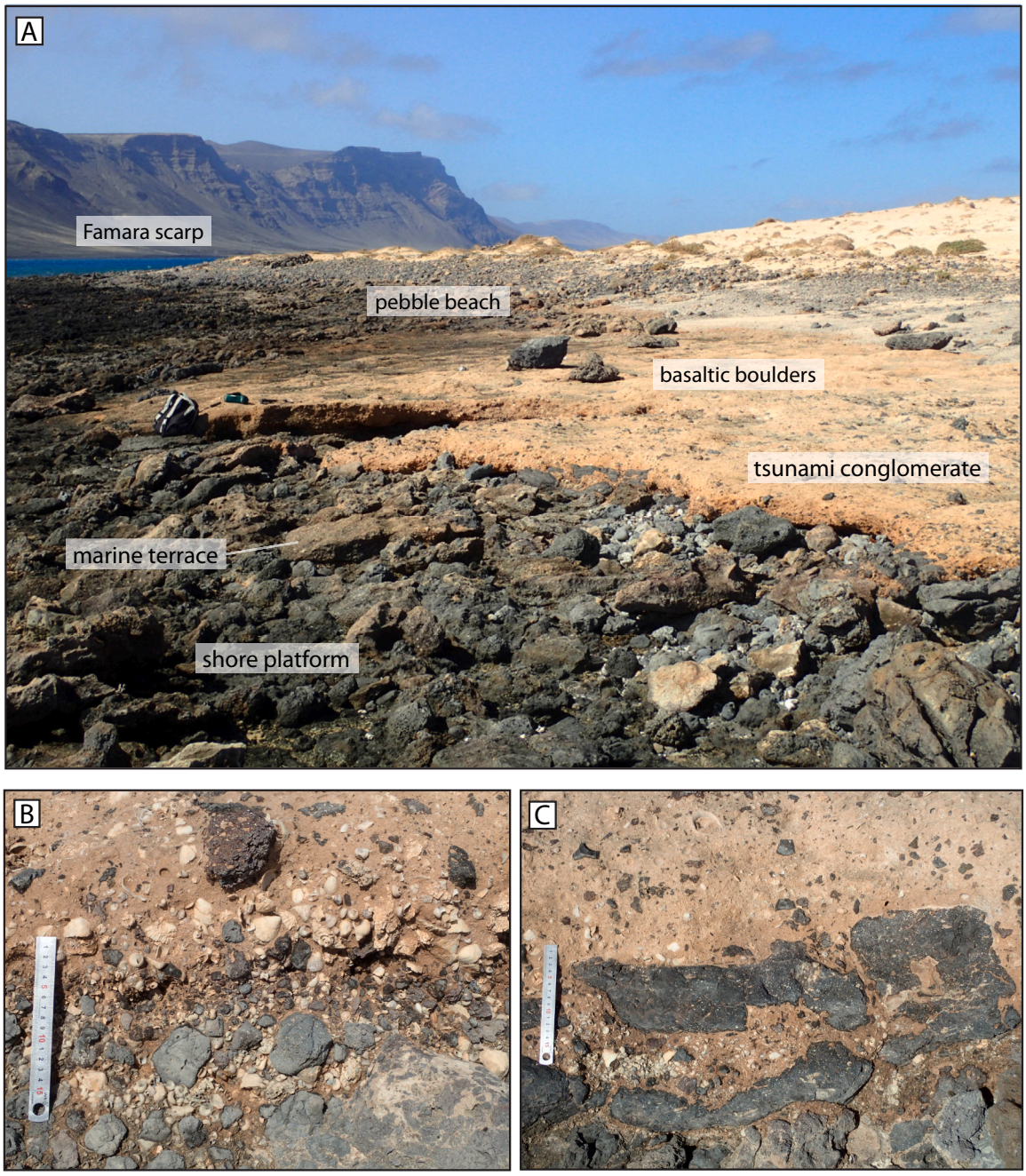

Fig. 3. Tsunami conglomerate overlying the rocky shore platform at Caleta del Aguardiente. A: general view of the site; B: cross-sectional view of the tsunami deposit, showing two subunits (lower subunit is clast-supported and rich in basaltic clasts, whereas upper subunit is matrix-supported, with more marine bioclasts and less basaltic clasts compared to the lower subunit); C: closer view to the erosional base, as evidenced by basaltic boulders from the shore platform embedded in the tsunami deposit.

before being converted into CO_2 by H_3PO_4 dissolution in under vacuum and reduced to graphite (Hatté et al., 2023). The graphite is then pressed and fitted into a target to be measured on the solid source of ECHoMICADAS (Tisnérat-Laborde et al., 2015). The *Patella* C14 12 underwent the same 0.1 N HNO_3 pre-treatment but was directly introduced as CO_2 to the ECHoMICADAS gas source through the CHS-GIS interface (Wacker et al., 2013). With the precision being lower with the gas source than with the solid source, two aliquots of 100 μg of C were measured. IAEA C1 and IAEA C2 are run at the same time than samples to check the quality of the handling process. $^{14}C/^{12}C$ ratio was normalized to Oxalic Acid 2 and reported as $F^{14}C$.

In order to translate the residual ^{14}C activities obtained from marine organisms into true years, it is necessary to define the so-called reservoir age (R_{sple}), *i.e.* the difference between the marine ^{14}C age and the atmospheric ^{14}C age. This reservoir age is estimated in two stages: the estimation of the global reservoir age of the open ocean (R_{global}) and the estimation of the local effect (ΔR), with $R_{sple} = R_{global} + \Delta R$. The most recent marine calibration curve, Marine20, proposes a R_{global} (R_{20}) varying with time and a ΔR (here ΔR_{20}) constant in time (Heaton et al., 2022). From the latter, we extracted data for Senegal-Mauritania (~17.0°N) and Morocco (7.4–8.7°N) coasts (Ndeye, 2008; Soulet et al., 2023), the two locations closest to La Graciosa for which a ΔR is reported in the "ΔR atlas" (Reimer and Reimer, 2001). They give ΔR_{20} equal to -63 ± 79 and $+ 180 \pm 289$ ^{14}C years, respectively, for shells collected between 1908 and 1948 CE. To ensure the reliability of the database, this atlas takes only into consideration the ^{14}C marine age

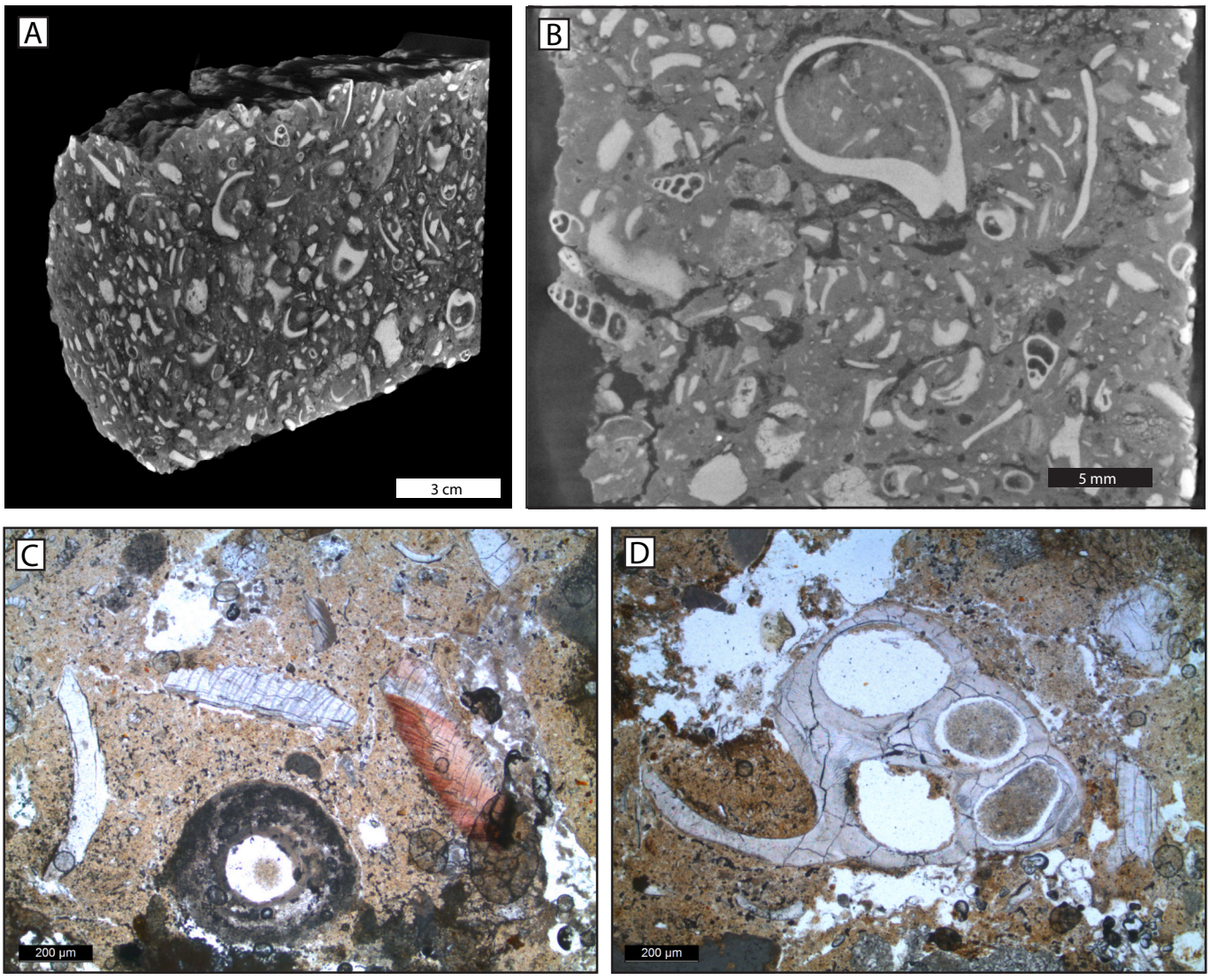

Fig. 4. X-ray tomography (A-B) and microscope (C—D) views of the tsunami conglomerate at Caleta del Aguardiente.

obtained on shells collected alive (recently or stored in museums). It therefore reflects the geographical diversity of current reservoir ages. However, the offset between the coastal environment and the open ocean fluctuates over time. Also, with a ΔR_{20} constant over time and equal to the current one, as proposed by the "ΔR atlas", it is not possible to represent the modulation of ΔR with time. We have therefore supplemented what is proposed by the "ΔR atlas" with a review of the literature. The ^{14}Canarias web application (Pardo-Gordó et al., 2023) that brings together all the ^{14}C dates obtained in an archaeological context in the Canary Islands, makes it possible to find data pairs with marine and atmospheric ^{14}C dating.

Among the available articles, two publications (Martins et al., 2012; Soares et al., 2011) refer to ten unambiguous pairs of ^{14}C dating that are compiled in Table 1. These dating pairs are based on ^{14}C dating on *Patella* as marine component and either on charred wood or animal bone as terrestrial component. Pairs including human bones have not been included as they are likely to be biased by a possible marine diet. The time range covered by these dating remains relatively restricted, extending from 130 to 950 BP. The reservoir ages, R, for all the individual pairs have been calculated and the deviation towards the global marine calibration (Marine20), ΔR_{20}, was extracted from the Reimer and Reimer (2017) online application. For two of the pairs, the application was unable to give a ΔR, the ages being too recent. The weighted average of individual ΔR_{20} was calculated and yielded for -78 ± 88 ^{14}C years, 88 ^{14}C years being the standard deviation between selected values.

3.3. Stable carbon and oxygen isotope measurements of mollusc shells

Three fragments were taken from the adult part of 17 individual Patella shells. These fragments were identified for each sample with the capital letters A, B and C (Table 3). Stable isotope compositions of the corresponding powders were determined using an auto sampler Multiprep™ coupled to a dual-inlet and a GV Isoprime® mass spectrometer. For each sample, an aliquot of about 400 µg of calcium carbonate was reacted with anhydrous oversaturated phosphoric acid at 90 °C during 20 min. Oxygen isotope ratios of calcium carbonate were computed assuming an acid fractionation factor $1000\ln\alpha(CO_2\text{–}CaCO_3)$ of 8.1 between carbon dioxide and calcite (Swart et al., 1991). However, acid fractionation factors differ between aragonite and calcite as shown by Kim and O'Neil (1997) and Kim et al. (2007). At a temperature of 90 °C, the mean difference in acid fractionation factors between aragonite and calcite is +0.4 ‰ (Kim et al., 2007). Consequently, such offset value was applied to all mollusc oxygen isotope measurements as they all made of aragonite. For the use of the Grossman and Ku (1986)'s oxygen isotope fractionation equation, the δ^{18}O of seawater reported on the VSMOW

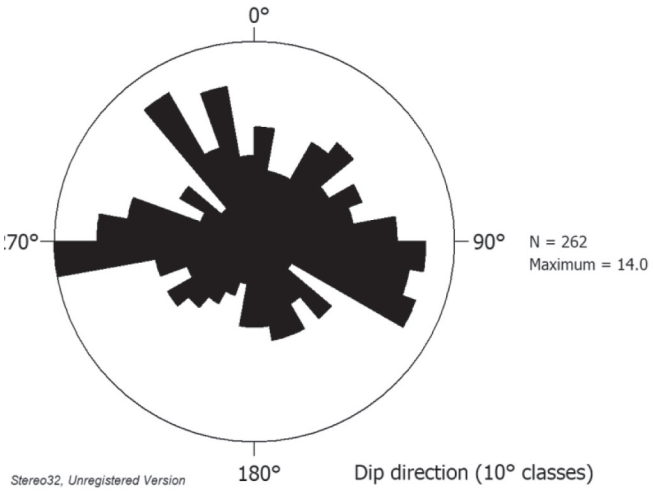

Fig. 5. Current orientation evidenced by azimuthal and dip-angle data of grains larger than 1 mm^3 (~fine sand to gravel size) in the tsunami conglomerate (Caleta del Aguardiente outcrop) illustrated as a rose diagram. (For interpretation of the references to colour in this figure legend, the reader is referred to the web version of this article.)

scale has been recalculated to fit the VPDB scale by applying the following equation: $\delta^{18}O_{(VPDB)} = \delta^{18}O_{(VSMOW)}$ -0.27 (Hut, 1987). All sample measurements were duplicated and adjusted to the international references NIST NBS18 ($\delta^{18}O_{VPDB} = -23.2$ ‰; $\delta^{13}C_{VPDB} = -5.01$ ‰), NBS19 ($\delta^{18}O_{VPDB} = -2.20$ ‰; $\delta^{13}C_{VPDB} = +1.95$ ‰), and an internal standard of Carrara marble ($\delta^{18}O_{VPDB} = -1.84$ ‰; $\delta^{13}C_{VPDB} = +2.03$ ‰). External reproducibility was close to ±0.1 ‰ for $\delta^{18}O$ and ± 0.05 for $\delta^{13}C$ (2σ).

4. Results

The results presented below confirm that the marine conglomerate briefly described by Galindo et al. (2021) is indeed a tsunami deposit. The main outcrops of tsunami deposits are located in the intertidal and supratidal zones along the eastern coast of La Graciosa Island, but we also found evidence of tsunami runup further inland. We thus distinguish between: (1) a proximal trace of tsunami that consists of a fossil-bearing conglomerate in the intertidal-supratidal zones, and (2) a distal trace corresponding to rounded basaltic pebbles and marine shells dispersed on slopes at altitudes up to 21 m above the present-day sea level. We have found no evidence of similar tsunami deposits other than on the east coast.

4.1. Structure and composition of the tsunami conglomerate

The proximal tsunami deposit is a poorly-sorted polymictic conglomerate up to 50 cm thick, overlying either Upper Pleistocene (locally known as Jandian: García-Talavera, 2002) aeolianites (Fig. 2: Punta Corrales), on residuals of a marine terrace at +0.2 m a.s.l. (to which García-Talavera, 2002, attributes a Holocene-Erbanian age) or directly on basaltic lava flows exposed on a shore platform (Fig. 3:).The +0.2 m a.s.l. marine terrace is particularly well-exposed on the shore platform between Caleta del Aguardiente and Caleta del Sebo (Fig. 1).

The basal contact with the substratum is erosional, and it slightly dips seaward. At Caleta del Aguardiente, erosion by the incoming tsunami is evidenced by large clasts of basalt ripped from the shore platform and buried in the lower part of the conglomerate. As observed on the field, thin sections and X-CT imagery (Fig. 4), the lithology of the clasts shows a great diversity: basaltic clasts (up to 2.2 m large boulders), beach rock, marine calcarenite, aeolianites, marine bioclasts (calcareous algae, bivalve and gastropod shells, sea worms), terrestrial bioclasts (snails, *Anthophora* nests, ovicaprid bones), and ceramics. Many shells are fragmented. This mixed marine-terrestrial composition is one of the

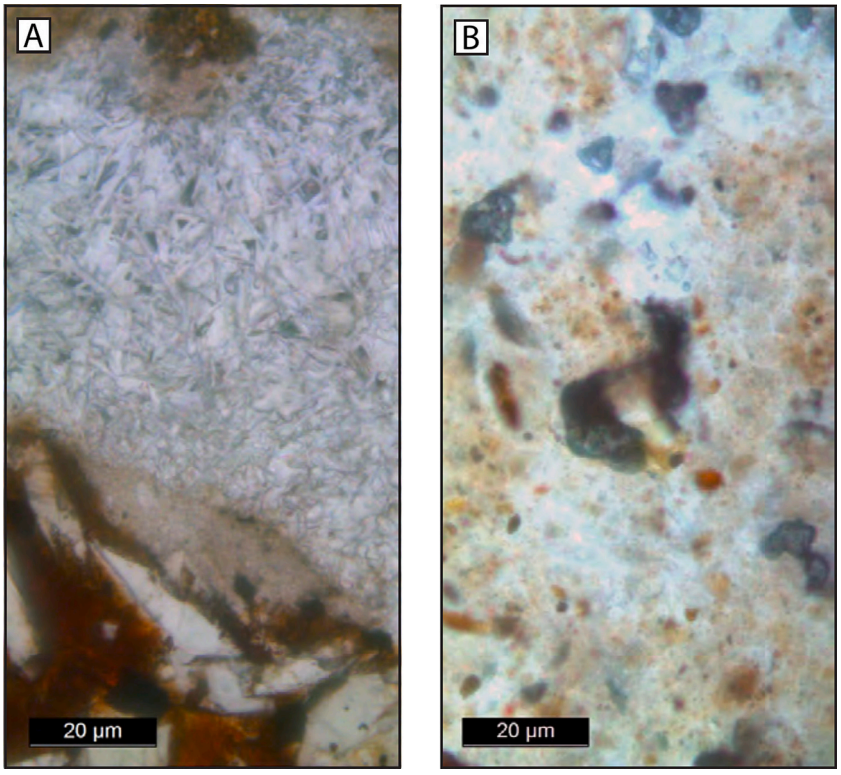

Fig. 6. Contrasting development of carbonate coating (calcrete) in (A) a Holocene marine terrace (0 m a.s.l.), and (B) a tsunami conglomerate (+0.2 m a.s.l.) on the eastern coast of La Graciosa (Caleta del Aguardiente).

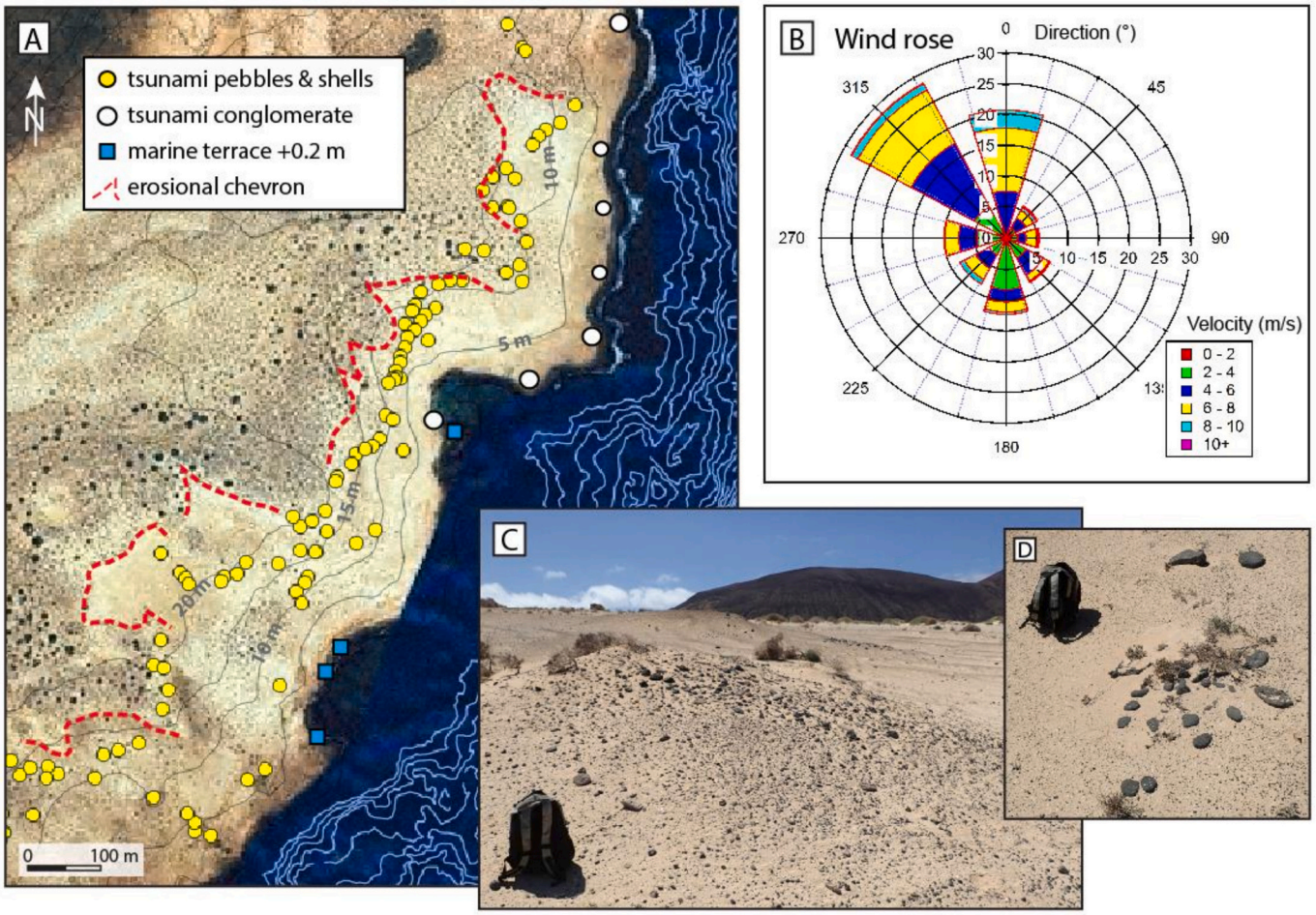

Fig. 7. Tsunami runup on the eastern coast of La Graciosa Island as evidenced by A: tsunami deposits and erosional chevrons in aeolian deposits; B: wind rose of the Órzola station in North Lanzarote (calculated from 2023 and 2024 data downloaded from https://metrics.grafcan.es); C: patches of basaltic rounded pebbles dispersed on slopes at altitudes up to 21 m inside the chevrons; D: closer view to the pebbles. Contour lines each 5 m for the topography and 1 m for the bathymetry. (For interpretation of the references to colour in this figure legend, the reader is referred to the web version of this article.)

criteria used to distinguish tsunami deposits from other types of deposits, such as storm deposits or raised marine terraces, although the distinction is not always so easy to make (Cuven et al., 2013; Paris et al., 2018; Engel et al., 2020).

The great majority of the macroscopic clasts fall in the pebble size fraction. The largest clasts (cobbles and boulders) are sometimes imbricated, thus preserving both a landward current direction in the lower part of the deposit and a seaward current direction in its upper part.

The matrix is made of silt-to-sand size calcarenite and aeolianite with abundant marine and terrestrial fossil fragments (Fig. 2). In certain places, we can distinguish between a lower clast-supported subunit, particularly rich in large clasts of basalt, and an upper matrix-supported subunit with abundant aeolianite (Fig. 3). The sedimentary fabric in the upper subunit is anisotropic, showing a clear preferred orientation of the grains in the matrix (Fig. 5). The bimodal pattern of the rose diagram does not allow for inferring a current direction, but the NW-SE orientation is concordant with a flow roughly transverse to the shoreline. The presence of terrestrial bioclasts (*e.g.*, snails) and abundant sand from the aeolian deposits upslope rather suggests a backwash (outflow) deposit.

The tsunami conglomerate is strongly cemented in the intertidal zone, and weakly cemented in the supratidal zone. The cement is a micritic carbonate coating draping the grains (Fig. 6). This poorly-developed calcrete contrasts with the microsparitic, locally needle-shaped, cementation that characterizes the +0.2 m a.s.l. marine terrace. Previous work has shown that the formation of carbonate cement in intertidal sedimentary formations can be very rapid when conditions are favourable, as demonstrated by the presence of beachrocks on historical lava flows at La Palma, Canary Islands (Calvet et al., 2003).

4.2. Spatial distribution of rounded pebbles and marine shells

Landward on the slopes covered by aeolian sands, we found numerous patches of rounded pebbles of basalt and shells (Fig. 7). The vast majority of the shells are those of terrestrial snails mixed with marine gastropods (*Patella* and various Muricidae), fragments of bivalve and worm shells (Vermitidae). The rounding of the clasts indicates a coastal origin (pebble beach), given the absence of fluvial systems on the island. The mean size of the pebbles decreases landward, from very coarse (>32 mm) to medium pebbles (8–16 mm). Their spatial distribution follows the present-day topography, with a maximum altitude exceeding 15–20 m in the topographic lows, and 10–15 m on the headlands. In fact, the patches of rounded pebbles and marine shells are associated to a morphology of en-echelon chevrons that is particularly well-preserved between Caleta de Aguardiente and Pedro Barba (Figs. 1 & 7). The chevrons have irregular contours compared to the U- and V-shaped coastal chevrons described in the literature (*e.g.*, Vimpere et al., 2019), but are clearly distinguishable on satellite images as they are almost devoid of vegetation (Fig. 7). They are between 180 and 300 m wide, opening out to the southeast, and extend 150 to 400 m inland, at an altitude of 15 to 25 m. The two most pronounced chevrons are

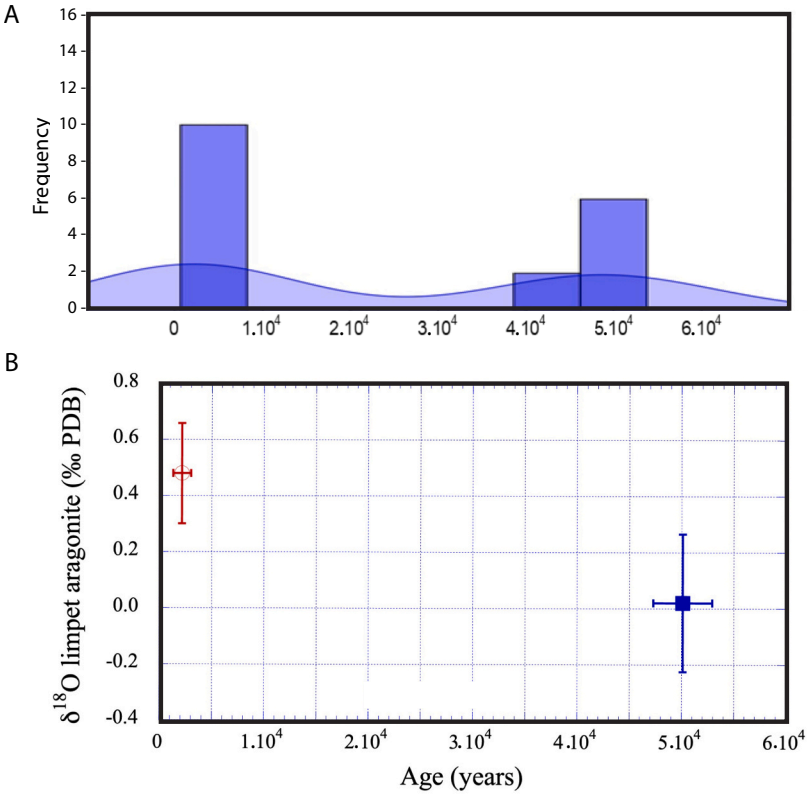

Fig. 8. (A) Kernel density diagram of ^{14}C dates showing two distinct clusters (B) and their respective mean $\delta^{18}O$ values.

located in the axis of two small bays (Fig. 7).

4.3. ^{14}C dating of the mollusc shells

The ^{14}C dating results fall into two main groups (Fig. 8): (1) a first group ranging from the ^{14}C dating limit to 44.2 cal kBP, and (2) a second group from 3200 cal BP to the pre-bomb period. The second group can be subdivided into subgroups: a subgroup around 3000 cal BP, another one around 1500 cal BP, and (3) a third subgroup extending from 500 to 200 cal BP, although these subdivisions are not statistically well-defined (Fig. 9).

In details, mollusc shells of the "old" group of ages were all sampled in the tsunami conglomerate (Caleta del Aguardiente), except one that comes from cemented aeolian deposits (GifA22482 in Table 2), whose Upper Pleistocene age is thus confirmed.

Shells from the "young" group were collected in different environments. Shells embedded in the calcrete of the +0.2 m a.s.l. marine terrace yield two ages around 3000 cal BP (Table 2 and Fig. 9: samples GifA22479 and GifA22480), which is concordant with similar marine terraces at 0–0.2 m a.s.l. dated between 3500 and 2700 cal BP on the northern coast of Fuerteventura (Zazo et al., 2002).

Shells sampled in the patches of rounded pebbles inside the erosional chevrons have ages between 2500 cal BP and 300 cal BP, without any spatial logic that might reflect long-term processes. The youngest age (sample GifA22481: 185 cal BP median age, 379 cal BP maximum age) is obtained on a shell collected in aeolian deposits that are truncated by an erosional chevron at Caleta del Aguardiente.

4.4. Stable isotope data

Fifty-one samples collected from 17 aragonitic gastropod shells (*Patella*) have been analyzed for their stable carbon and oxygen isotope compositions (Table 3). Their $\delta^{13}C$ and $\delta^{18}O$ values range from 0.83 ‰ to 5.77 ‰ (VPDB) and from −0.30 ‰ to 1.01 ‰ (VPDB). When these isotopic ratios are reported against the two main groups of ^{14}C dates according to a Kernel density diagram (Fig. 8), two distinct clusters are defined according to the results provided by a Wilcoxon Mann-Whitney test ($p = 1.56 \times 10^{-3}$ for $\delta^{18}O$ and $p = 0.114$ for $\delta^{13}C$; Ho = identical distributions). The young ^{14}C-based cluster (≈ 3.2–0.3 cal kBP) is characterized by mean $\delta^{13}C$ (3.40 ± 1.27 ‰) and $\delta^{18}O$ (0.48 ± 0.18 ‰) values which are both higher than those of the oldest cluster (≈ 40–50 cal kBP) with $\delta^{13}C$ and $\delta^{18}O$ values of 2.22 ± 1.01 ‰ and 0.02 ± 0.24, respectively (Table 3; Fig. 8).

5. Discussion

5.1. Age of the tsunami

If we rely on the ^{14}C ages obtained from the *Patella* shells from the conglomerate, the tsunami would have occurred around 50 kyrs ago. However, this is in contradiction with certain eustatic, stratigraphic, and geomorphological arguments that suggest a much more recent event. First, the sea level around 50,000 BP was much lower (of the order of 70–80 m) than the current level (Spratt and Lisiecki, 2016), given that the eastern Canary Islands have remained relatively stable since the Late Pleistocene. If we assume that Lanzarote did not experienced significant uplift or subsidence during the last 50 kyrs (Zazo et al., 2002), we must imagine an extreme event capable of transporting marine shells over ~10 km, a distance that separates their current location at 5–20 m a.s.l. from the −80 m isobaths northeast of La Graciosa. Only a gigantic tsunami generated by a massive island flank collapse could cause such a runup, but no event of this type is recorded in the eastern Canary Islands around 50,000 BP (Paris et al., 2018; Costa et al., 2021).

In fact, the *Patella* shells of the "old" group of ^{14}C ages are most probably older than the tsunami itself, the latter having reworked the shells, whose origin remains undetermined at this stage. The tsunami

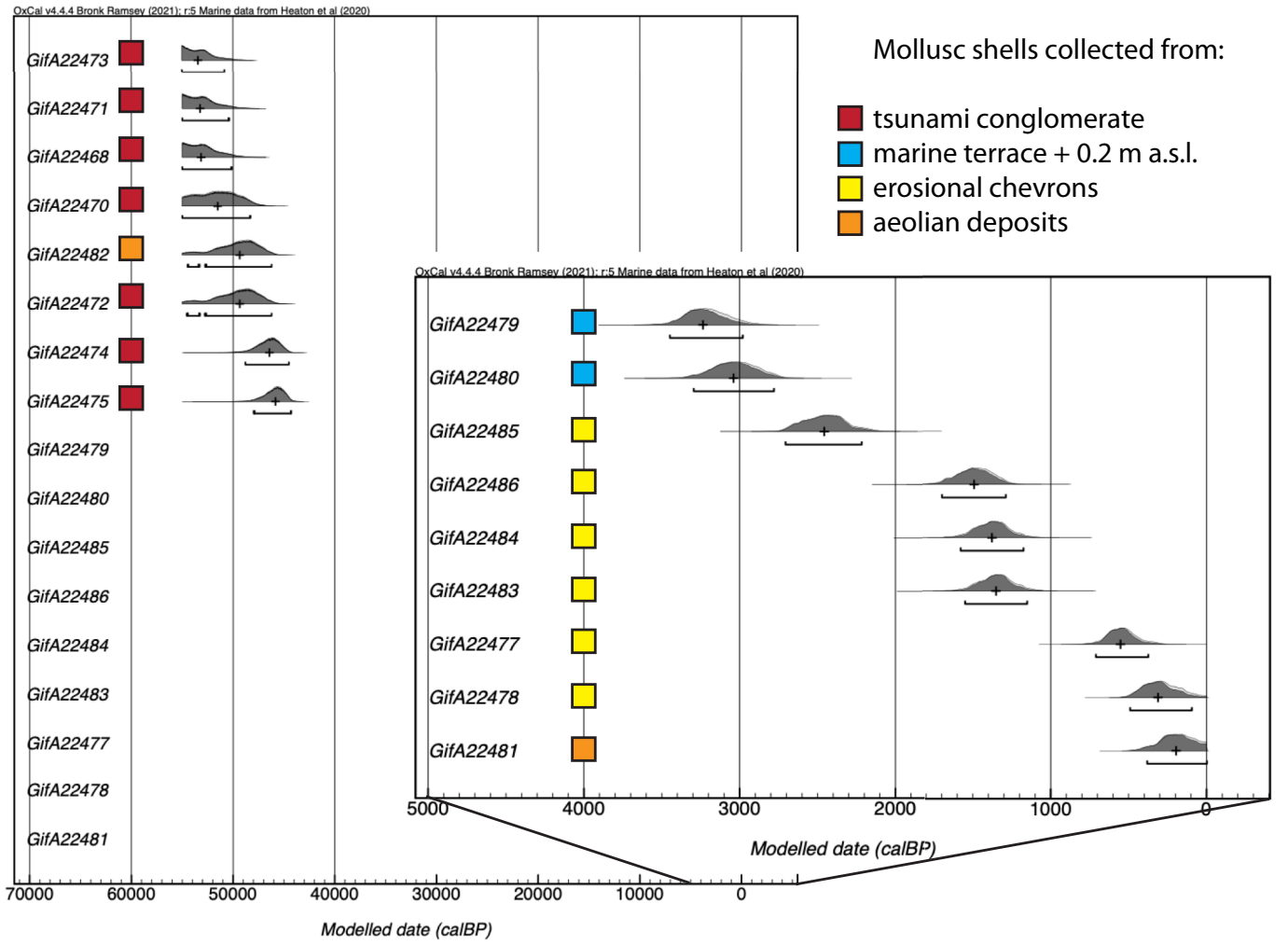

Fig. 9. Calibrated ^{14}C results on mollusc shells from La Graciosa Island, showing an old group of ages ranging from the ^{14}C dating limit to 44.2 cal kBP (left panel), and a young group (zoom panel on the right) from 3400 to 200 cal BP. Dating are identifiable thanks to the GifA- number (see Table 2).

conglomerate rests locally on the +0.2 m a.s.l. marine terrace in which we have dated two *Patella* shells at 3200–3000 cal BP (Fig. 9). This is concordant with (1) the age of 1730 ± 30 BP reported by Galindo et al. (2021) on a goat tooth found inside the tsunami conglomerate, and (2) the range of ages obtained from *Patella* shells collected in the chevrons (2500–300 cal BP). Chevron landforms observed all around the world have been the subject of debate as to their origin: aeolian processes, storms, or tsunamis (Maxwell and Haynes, 1989; Hearty et al., 1998; Scheffers et al., 2008; Bourgeois and Weiss, 2009; Gusiakov et al., 2009; Vimpere et al., 2019). The chevrons we describe here at La Graciosa are smaller (10^1–10^2 m scale) than the large chevrons (10^2–10^3 m) that were the subject of the controversy. They are very similar in size and shape to the chevrons described by Paris et al. (2009), (see their Fig. 7) on the coast of Lhok Nga, Indonesia, after the December 26, 2004 tsunami. Another argument that does not support a long-term wind-related process is the fact that the chevrons are oriented opposite to the dominant wind direction in northern Lanzarote. Indeed, they are opened to the south-east, whereas the dominant winds come from the NNW (Fig. 7B). We thus conclude that these chevrons attest to a morphogenic event having excavated the Upper Pleistocene aeolian deposits. Not only is the morphological imprint fresh in the landscape, but the vegetation is also far less developed within the chevrons, which implies a quite recent event.

The Caleta de Sebo has regularly been used as a first anchorage by navigators from Europe since the 14th century. It is difficult to imagine that a tsunami flooding the entire eastern coast of La Graciosa could have remained ignored in all available archives. The tsunami must therefore have occurred shortly or at the very beginning of European colonization, at a time when La Graciosa was not often visited (end of the 13th century or beginning of the 14th century).

5.2. *Source of the Patella shells as inferred from $\delta^{18}O$ values*

Stable isotope data provide some insight into the source of the *Patella* shells dated around 50,000 BP. Using the oxygen isotope fractionation equation established by Grossman and Ku (1986) for marine molluscs, *Patella* samples assigned to the "young" group of ^{14}C ages (3.2–0.2 cal kBP) provide seawater temperatures of 22.1 ± 0.8 °C, slightly higher than the recorded present-day (21.2 °C; Meco et al., 2018) or pre-industrial sea surface temperature of 19.4 ± 0.1 °C calculated by Maréchal et al. (2020) for the Canary Archipelago. Such temperatures have been calculated assuming a seawater $\delta^{18}O$ value of +1.1 ‰ (VSMOW) similar to the composition of modern Lanzarote and Fuerteventura coastal marine waters (Clauzel et al., 2019). The hypothesis is robust, as the $\delta^{18}O$ value of a water mass reflects its hydrological budget, which is considered to be in a steady state for at least 6000 years in the Mediterranean Sea (Emeis et al., 2003). Higher $\delta^{13}C$ values recorded by the shells of the young group (3.2–0.2 cal kBP) could reflect a higher marine productivity compared to the old group (supposedly 40–50 cal kBP), perhaps in relation to changes in the upwelling activity located today around the Canary Archipelago.

Regarding the seawater temperatures inferred from the "old" group

Table 2
^{14}C ages obtained on Patella – Sample ID, lab ID, raw data as $F^{14}C$ and conventional age [1] (rounded according to Stuiver and Polach, 1977) and calibrated data on Marine20 (Heaton et al., 2020) with a $\Delta R_{20} = -78 \pm 88$ ^{14}C years using OxCal4.4 software (Bronk Ramsey, 2009) are provided. The calibrated ranges associated with a star (*) are beyond the calibration curve, either older or younger than the calibration curve limits.

Identification			Physical measurements				Calibrated ranges	
			raw data					
sample ID	chemistry #	measure #	$F^{14}C$	+ − 1 s	age [BP] [1]	±	95 % ranges	median
Ca-14 2 Patella indet.	GifA22468	ECHo-5325	0.0015	0.0005	52,200	2800	* 55002BP (95.1 %) 50242BP 50237BP (0.2 %) 50198BP 50176BP (0.1 %) 50158BP	
Ca-14 3 Patella indet.	GifA22469	ECHo-5326			$T > 52,200$			
Ca-14 4 Patella indet.	GifA22470	ECHo-5327	0.0023	0.0005	48,700	1800	* 55002BP (95.2 %) 48356BP 48352BP (0.1 %) 48337BP	
Ca-14 5 Patella indet.	GifA22471	ECHo-5328	0.0014	0.0005	53,000	3150	* 55002BP (95.4 %) 50340BP	
Ca-14 6 Patella indet.	GifA22472	ECHo-5329	0.0029	0.0005	46,900	1450	* 54492BP (0.1 %) 54468BP 54438BP (4.8 %) 53358BP 53300BP (0.2 %) 53238BP 53220BP (0.2 %) 53174BP 52730BP (90.2 %) 46218BP	
Ca-14 7 Patella indet.	GifA22473	ECHo-5330	0.0012	0.0005	53,800	3400	* 55002BP (95.2 %) 50782BP 50743BP (0.1 %) 50722BP 50712BP (0.1 %) 50692BP	
Ca-14 8 Thais haemastona	GifA22474	ECHo-5331	0.0039	0.0005	44,500	1100	48768BP (95.4 %) 44518BP	46,419
Ca-14 9 Thais haemastona	GifA22475	ECHo-5332	0.0042	0.0005	44,000	1050	47916BP (0.1 %) 47894BP 47886BP (95.3 %) 44296BP	45,825
Ca-11 11 Patella indet.	GifA22477	ECHo-5334	0.8786	0.0023	1040	20	712BP (95.4 %) 370BP	544
Ca-11 12 Patella indet.	GifA22478	ECHo-5335	0.9103	0.0024	755	20	492BP (95.4 %) 90BP *	292
Ca-12 13 Patella indet.	GifA22479	ECHo-5427	0.6530	0.0020	3425	25	3450BP (95.4 %) 2975BP	3212
Ca-12 14 Patella indet.	GifA22480.2 GifA22480.3	ECHo-5428.2.1 ECHo-5428.2.2	0.6655	0.0036	3270	45	3292BP (95.4 %) 2772BP	3025
Ca-15 15 Patella indet.	GifA22481	ECHo-5429	0.9226	0.0025	645	20	379BP (95.4 %) -2BP *	185
Ca-15 16 Patella indet.	GifA22482	ECHo-5430	0.0029	0.0005	46,800	1400	* 54479BP (0.3 %) 54400BP 54393BP (4.7 %) 53328BP 52726BP (90.2 %) 46249BP 46244BP (0.2 %) 46194BP	49,336
Ca-20 17 Patella indet.	GifA22483	ECHo-5431	0.7925	0.0022	1870	25	1550BP (95.4 %) 1148BP	1346
Ca-20 18 Patella indet.	GifA22484	ECHo-5432	0.7900	0.0023	1895	25	1580BP (95.4 %) 1170BP	1373
4 19 Patella indet.	GifA22485	ECHo-5433	0.7070	0.0020	2785	25	2705BP (95.4 %) 2206BP	2449
P-5 20 Patella indet.	GifA22486	ECHo-5434	0.7795	0.0021	2000	20	1702BP (95.4 %) 1286BP	1483

of *Patella* shells, the lower $\delta^{18}O$ values suggest similar or higher temperatures depending on the considered continental ice volume (Table 4). In any case, the temperatures inferred from those samples would be attributed to either a warm interval during the last glacial stage or to a previous interglacial stage, both consistent with the need for a sea level high enough to generate a marine terrace. The calculated ^{14}C dates ranging from 40 to 50 cal kBP could thus be older considering that we are at the limit of the dating method (Reimer et al., 2009). According to Guo et al. (2019), modeled MIS3 sea surface mean temperatures in the eastern Central Atlantic Ocean were about 1 °C to 2 °C lower than during the Pre-Industrial value of 19.4 °C, which was estimated by Maréchal et al. (2020) in the same geographic area. The "old" *Patella* shells could therefore be assigned to MIS5e (129 to 116 kBP), a stage that is characterized by a high sea level, high SST between 20.4 ± 1.3 °C and 22.2 ± 1.2 °C and a seawater $\delta^{18}O$ value estimated to be less than −0.1 relative to the present (Maréchal et al., 2020). Indeed, considering a seawater $\delta^{18}O$ value of 1.0 instead of 1.1, the derived temperature is calculated to be 23.7 ± 1.0 °C (Table 4).

We thus suggest that the *Patella* shells dated ~50 kBP using ^{14}C are in fact older, dating back to a warm interval of the last glacial stage or an interglacial stage, the MIS5e (124–119 kBP) being a likely candidate. Following this hypothesis, the tsunami would have eroded an old marine terrace, whose shells represent the great majority of the bioclastic content of the tsunami conglomerate. There is no published evidence of a MIS5e terrace on the eastern coast of La Graciosa Island, but the cemented aeolian deposits in which the chevrons are cut have a Upper Pleistocene age (García-Talavera, 2002). On the northwestern coast of Lanzarote (Zazo et al., 2002), the MIS5e terrace is exposed at +1.5 m a.s.l. During our survey to the western coast of La Graciosa, we found an elevated shore platform at +1–1.5 m a.s.l. topped inland by a boulder ridge. Our interpretation is in line with the observations of García-Talavera (2002) on the great diversity and biotope mixing of the malacological fauna found in the tsunami conglomerate. García-Talavera, 2002 did not distinguish between the Holocene marine terrace at +0.2 m a.s.l. and the tsunami conglomerate, but he questioned the presence of gastropod species such as *Acanthina dontelei* and *Strombus latus*, which are usually found in MIS5e deposits.

5.3. A local landslide as a source of the tsunami?

Based on the single ^{14}C age (1730 ± 30 BP, 244–387 CE) they obtained in the tsunami deposit, Galindo et al. (2021) proposed the 382 CE earthquake as a possible source of the La Graciosa tsunami. This M 7.5 earthquake had an epicenter SW off Portugal, and its tsunami is included in the Portuguese and Moroccan catalogues (Baptista and Miranda, 2009; Kaabouben et al., 2009). However, the ~20 m tsunami runup inferred from the spatial distribution of tsunami deposits on the eastern coast of La Graciosa (Fig. 10) is not compatible with such a far-field earthquake source. As an example, the transatlantic tsunami generated by the November 1st, 1755 Lisbon earthquake caused wave runups less than 5 m high in the Canary Islands (Galindo et al., 2021).

Only a local source, such as a submarine landslide or a cliff collapse, could generate waves inundating the eastern coast of La Graciosa to altitudes up to 21 m. A relatively fresh landslide scar on the northern end of the Famara cliff, on the western coast of Lanzarote and facing the eastern coast of La Graciosa, could represent a good candidate (Fig. 10). The amphitheater-shaped scar is now partly filled by scree deposits. Considering the dimensions of the scar (430 × 420 m) and the height of

Table 3
Stable carbon and oxygen isotope compositions of aragonitic gastropod shells (*Patella sp.*).

Sample name	$\delta^{13}C$ (VPDB)	S.D.	$\delta^{18}O$ (VPDB)	S.D.
22468 A	2.790	0.031	0.101	0.019
22468B	2.605	0.126	0.312	0.045
22468C	4.268	0.023	0.567	0.055
22470 A	1.925	0.029	−0.142	0.041
22470B	1.825	0.090	−0.195	0.024
22470C	2.386	0.217	−0.124	0.012
22471 A	0.962	0.062	−0.040	0.095
22471B	1.013	0.000	−0.209	0.013
22471C	0.832	0.110	−0.101	0.035
22472 A	1.704	0.066	−0.219	0.014
22472B	1.721	0.005	0.123	0.045
22472C	1.750	0.004	−0.124	0.016
22473 A	3.977	0.151	0.267	0.112
22473B	3.546	0.035	0.148	0.105
22473C	3.450	0.055	0.189	0.014
22474 A	1.218	0.069	−0.287	0.028
22474B	1.504	0.050	−0.277	0.084
22474C	1.466	0.051	−0.177	0.039
22475 A	1.415	0.131	−0.302	0.132
22475B	1.816	0.016	0.019	0.006
22475C	1.382	0.181	−0.229	0.074
22477 A	5.425	0.001	0.628	0.055
22477B	5.690	0.093	0.781	0.007
22477C	5.774	0.035	1.012	0.116
22478 A	4.292	0.134	0.466	0.057
22478B	4.384	0.112	0.297	0.093
22478C	4.578	0.051	0.165	0.054
22479 A	2.713	0.001	0.557	0.025
22479B	2.749	0.075	0.467	0.048
22479C	3.283	0.050	0.029	0.008
22480 A	1.883	0.055	0.318	0.024
22480B	1.948	0.044	0.312	0.063
22480C	1.452	0.086	0.689	0.106
22481 A	4.724	0.127	0.284	0.147
22481B	4.796	0.018	0.398	0.063
22481C	4.873	0.070	0.386	0.025
22482 A	3.315	0.127	0.403	0.010
22482B	3.102	0.090	0.279	0.030
22482C	3.336	0.064	0.450	0.008
22483 A	3.085	0.024	0.514	0.011
22483B	3.160	0.008	0.663	0.029
22483C	3.168	0.052	0.659	0.042
22484 A	2.393	0.030	0.762	0.066
22484B	2.222	0.066	0.684	0.051
22484C	2.489	0.059	0.591	0.014
22485 A	2.539	0.091	0.359	0.093
22485B	3.444	0.013	0.302	0.054
22485C	3.071	0.043	0.528	0.033
22486 A	2.565	0.036	0.353	0.002
22486B	2.545	0.077	0.385	0.074
22486C	2.572	0.066	0.255	0.109

Table 4
Calculated seawater temperatures for the "young" *Patella* shells (3.2–0.3 kyr) considering the modern seawater $\delta^{18}O$ value of 1.1‰ (VSMOW) or 0.83‰ (VPDB) that was measured off Lanzarote and Fuerteventura (Clauzel et al., 2019). Seawater temperatures for the "old" *Patella* samples (40–50 kyr) were calculated for different $\delta^{18}O$ values of seawater reflecting the volume of continental ice, including a $\delta^{18}O$ value of 1.0‰ that corresponds to the composition of seawater during the MIS5e of the Last Interglacial (Maréchal et al., 2020).

Age	$\delta^{18}O$ *Patella*	$\delta^{18}O$ sw	$\delta^{18}O$ sw	T seawater	SD
(kyr)	VPDB	VSMOW	VPDB	°C	
				Grossman and Ku (1986)	
40–50	0.02	0.25	−0.02	**20.4**	**1.0**
	0.02	0.50	0.23	**21.5**	**1.0**
	0.02	0.75	0.48	**22.6**	**1.0**
	0.02	1.00	0.73	**23.7**	**1.0**
3.2–0.3	0.48	1.10	0.83	**22.1**	**0.8**

the cliff (320 m), we estimate a landslide volume of 7×10^6 m^3.

For comparison, a 2.87×10^6 m^3 cliff collapse in 1930 in Madeira generated a deadly tsunami with wave heights up to 5 m and an inundation distance up to 110 m on the nearest populated coast (Omira et al., 2022). Another cliff collapse in Flores Island, Azores, triggered a tsunami with a runup of 5–7 m in 1857, causing the death of 10 people on the coasts of Flores and Corvo (Cabral, 2009). More recently, a small cliff collapse in La Gomera on November 14, 2020, generated a 0.5-m-high wave on a beach located 200 m away (Galindo et al., 2021).

In the case of La Graciosa, the cliff collapse scar is located just in front of the largest chevrons and highest tsunami deposits (~20 m a.s.l.), *i.e.* where the tsunami runup was greatest. The maximum altitude of the tsunami deposits decreases rapidly with distance from the collapse (< 4 m a.s.l. at 4 km).

6. Conclusions

This study questions the reliability of ^{14}C dating of event deposits (tsunamis, storms, floods, *etc.*) based on dating of material contained in the deposits and therefore having been transported from different sediment sources. Only an exhaustive approach, based on a large number of ages both in the deposits and in the different sedimentary environments that fed the tsunami, can constrain its age. This question is particularly crucial in arid environments where marine bioclasts represent the only datable material.

The supposed source of the tsunami is a collapse of the Famara coastal cliff in the Strait of El Rio, which separates La Graciosa from Lanzarote, just opposite to the outcrops of tsunami deposits and to the maximum runup of the tsunami. The reconstructed tsunami runups of over 20 m underlines the fact that this hazard type should not be neglected. The permanent population of La Graciosa is currently close to 1000 inhabitants who live in the harbor of Caleta del Sebo, located in the southeast part of the island. In recent decades, the economy of La Graciosa island shifted from a model based on agriculture and fishing to one based on tourism. Most of the people are concentrated around Caleta de Sebo and the beaches to the South. The entire town and these beaches are located in the area that was flooded by the tsunami. In future work, it would be interesting to date the collapse scar to confirm its link with the tsunami, and to carry out numerical modelling coupling the landslide and the tsunami.

CRediT authorship contribution statement

Raphaël Paris: Writing – review & editing, Writing – original draft, Methodology, Investigation, Formal analysis, Conceptualization. **Franck Lavigne:** Writing – review & editing, Writing – original draft, Methodology, Investigation, Conceptualization. **Christine Hatté:** Writing – review & editing, Writing – original draft, Formal analysis. **Juan Francisco Betancort:** Writing – original draft, Conceptualization. **Jean-Pierre Flandrois:** Writing – original draft, Formal analysis. **Arnauld Vinçon-Laugier:** Writing – original draft, Formal analysis. **Eve Poulallion:** Writing – original draft, Formal analysis. **Simon Falvard:** Writing – original draft, Formal analysis. **Bachtiar W. Mutaqin:** Writing – original draft, Formal analysis. **Christophe Lécuyer:** Writing – review & editing, Writing – original draft, Project administration, Methodology, Investigation, Funding acquisition, Formal analysis, Conceptualization.

Declaration of competing interest

Raphael paris reports financial support was provided by Région AuRA. Christophe Lecuyer reports financial support was provided by CNRS MITI. If there are other authors, they declare that they have no known competing financial interests or personal relationships that could have appeared to influence the work reported in this paper.

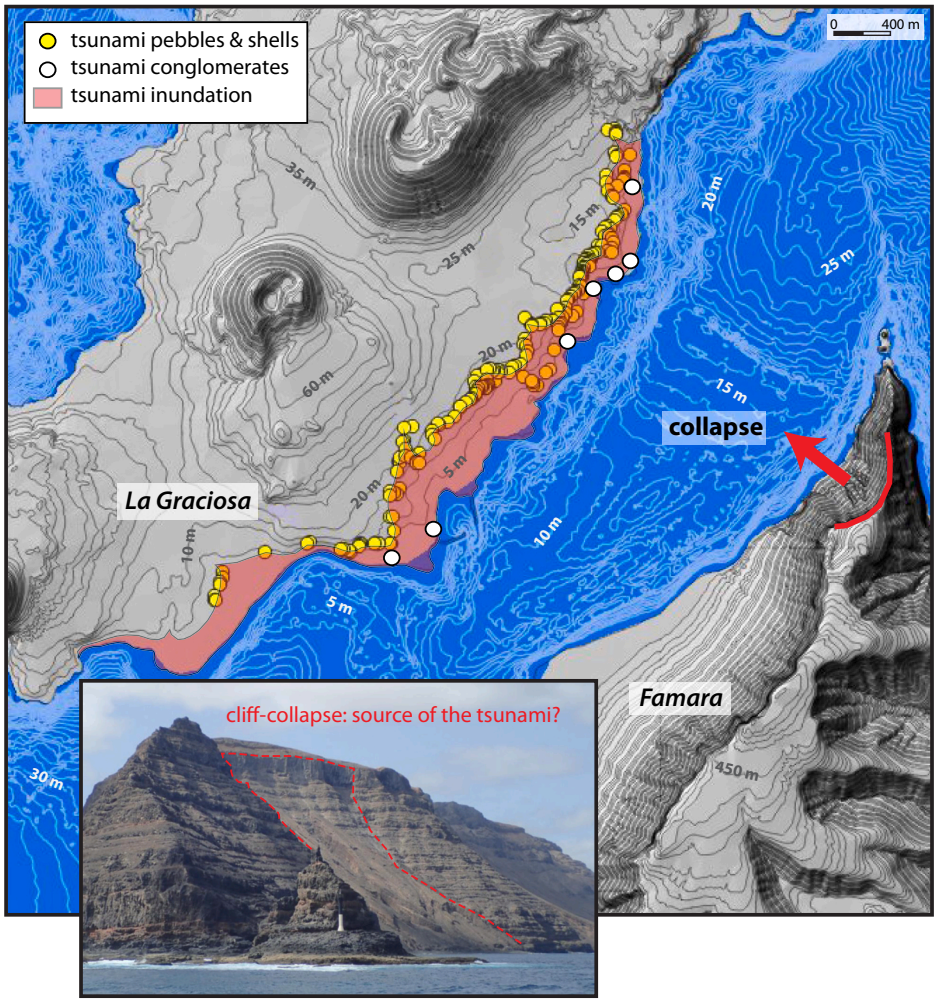

Fig. 10. Location map of tsunami deposits on the eastern and southern coasts of La Graciosa Island, Canary Islands. Red line and arrow indicate the landslide scar area on the western coast of the Famara massif, as a possible source of the tsunami. The red area represents the inundated area as inferred from the spatial distribution of the tsunami deposits (yellow dots). Contour lines each 5 m for the topography and 1 m for the bathymetry. Inset: Landslide scar of a cliff collapse on the western coast of the Famara massif, Lanzarote Island. (For interpretation of the references to colour in this figure legend, the reader is referred to the web version of this article.)

Acknowledgements

This work received financial support from the CNRS MITI Interdisciplinary Programme (THOLOC project led by Christophe Lécuyer) and the Région AuRA (CT-SCAM project led by Raphaël Paris). The authors are grateful to Aurélie Colomb (LaMP-UCA) for processing the wind data, and to the four reviewers, Ricardo Ramalho, Dave Tappin, and two anonymous reviewers for their relevant comments. This is ClerVolc contribution n° 707.

Data availability

All relevant data used for the research described in this article is permanently available in a public repository at https://www.opgc.fr/DOI/10.25519/x0hy-8c85/

References

Araoka, D., 2020. Radiocarbon and U/Th dating of tsunami- and storm-transported coarse clasts. In: Engel, M., Pilarczyk, J., May, S.M., Brill, D., Garrett, E. (Eds.), Geological Records of Tsunamis and Other Extreme Waves. Elsevier, pp. 663–685.
Baptista, M.A., Miranda, J.M., 2009. Revision of the Portuguese catalog of tsunamis. Natural Hazards and Earth Systems Science 9, 25–42.
Bourgeois, J., Weiss, R., 2009. "Chevrons" are not mega-tsunami deposits - a sedimentologic assessment. Geology 37, 403–406.
Brill, D., Tamura, T., 2020. Optically stimulated luminescence dating of tsunami and storm deposits. In: Engel, M., Pilarczyk, J., May, S.M., Brill, D., Garrett, E. (Eds.), Geological Records of Tsunamis and Other Extreme Waves. Elsevier, pp. 663–685.
Bronk Ramsey, C., 2009. Bayesian analysis of radiocarbon dates. Radiocarbon 51 (1), 337–360.
Cabral, N., 2009. Análise do Perigo de Tsunamis Nos Açores. Doctoral dissertation. Tese de Mestrado em Vulcanologia e Riscos Geológicos, Universidade, dos Açores.
Calvet, F., Cabrera, M.C., Carracedo, J.C., Mangas, J., Pérez-Torrado, F.J., Recio, C., Travé, A., 2003. Beachrocks from the island of La Palma (Canary Islands, Spain). Mar. Geol. 197, 75–93.
Carracedo, J.C., Day, S., Guillou, H., Rodriguez Badiola, E., Canas, J.A., Pérez Torrado, F. J., 1998. Hotspot volcanism close to a passive continental margin: the Canary Islands. Geol. Mag. 135 (5), 591–604.
Castro, N., Carlton, J.T., Costa, A.C., Marques, C.S., Hewitt, C.L., Cacabelos, E., Canning-Clode, J., 2022. Diversity and patterns of marine non-native species in the archipelagos of Macaronesia. Divers. Distrib. 28 (4), 667–684.
Clauzel, T., Maréchal, C., Fourel, F., Barral, A., Amiot, R., Betancort, J.-F., Lomoschitz, A., Meco, J., Lécuyer, C., 2019. Reconstruction of sea-surface temperatures in the Canary Islands during marine isotope stage 11. Quatern. Res. 1, 15.
Coello, J., Cantagrel, J.M., Hernán, F., Fúster, J.M., Ibarrola, E., Ancochea, E., Casquet, C., Jamond, C., Díaz, J.R., Cendrero, A., 1992. Evolution of the eastern volcanic ridge of the Canary Islands based on new K–Ar data. J. Volcanol. Geotherm. Res. 53, 251–274.
Costa, P.J., Dawson, S., Ramalho, R.S., Engel, M., Dourado, F., Bosnic, I., Andrade, C., 2021. A review on onshore tsunami deposits along the Atlantic coasts. Earth-Science Reviews 212, 103441.
Cuven, S., Paris, R., Falvard, S., Miot-Noirault, E., Benbakkar, M., Schneider, J.L., Billy, I., 2013. High-resolution analysis of a tsunami deposit: case-study from the 1755 Lisbon tsunami in southwestern Spain. Mar. Geol. 337, 98–111.

Damnati, B., Petit-Maire, N., Fontugne, M., Meco, J., Williamson, D., 1996. Quaternary paleoclimates in the eastern Canary Islands. Quat. Int. 31, 37–46.
de Teguise, Ayuntamiento, 1871. Reglamentación sobre la Administración del Islote Graciosa. Archivo Histórico de la Villa de Teguise.
Dominey-Howes, D., Cundy, A., Croudace, I., 2000. High energy marine flood deposits on Astypalaea Island, Greece: possible evidence for the AD 1956 southern Aegean tsunami. Mar. Geol. 163, 303–315.
Emeis, K.-C., Schulz, H., Struck, U., Rossignol-Strick, M., Erlenkeuser, H., Howell, M.W., Kroon, D., Mackensen, A., Ishiuka, S., Oba, T., Sakamoto, T., Koizumi, I., 2003. Eastern Mediterranean surface water temperatures and d18O composition during deposition of sapropels in the late quaternary. Paleoceanography 18 (1), 1005.
Engel, M., Pilarczyk, J., May, S.M., Brill, D., Garrett, E., 2020. Geological Records of Tsunamis and Other Extreme Waves. Elsevier, p. 848.
Galindo, I., Romero, C., Martín-González, E., Vegas, J., Sánchez, N., 2021. A review on historical tsunamis in the Canary Islands: implications for tsunami risk reduction. Geosciences 2021 (11), 222.
García-Talavera, F., 2002. Depósitos marinos fosilíferos del holoceno de La Graciosa (Islas Canarias) que incluyen restos arqueológicos. Revista de la Academia Canaria de Ciencias 14, 19–35.
Geldmacher, J., Hoernle, K., van den Boogard, P., Duggen, S., Werner, R., 2005. New $^{40}Ar/^{39}Ar$ age and geochemical data from seamounts in the Canary and Madeira volcanic provinces: support for the mantle plume hypothesis. Earth Planet. Sci. Lett. 237, 85–101.
Grossman, E.L., Ku, T.L., 1986. Oxygen and carbon isotope fractionation in biogenic aragonite: temperature effects. Chemical Geology: Isotope Geoscience Section 59, 59–74.
Guo, C., Nisancioglu, K.H., Bentsen, M., Bethke, I., Zhang, Z., 2019. Equilibrium simulations of marine isotope stage 3 climate. Clim. Past 15 (3), 1133–1151.
Gusiakov, V., Abbott, D., Bryant, E.A., Masse, W., Breger, D., 2009. Mega Tsunami of the world oceans: chevron dune formation, micro-ejecta, and rapid climate change as the evidence of recent oceanic bolide impacts. In: Beer, T. (Ed.), Geophysical Hazards. Springer, Netherlands, Dordrecht, pp. 197–227.
Hatté, C., Arnold, M., Dapoigny, A., Daux, V., Delibrias, G., Du Boisgueheneuc, D., Fontugne, M., Gauthier, C., Guillier, M.-T., Jacob, J., Jaudon, M., Kaltnecker, E., Labeyrie, J., Noury, C., Paterne, M., Pierre, M., Phouybandhyt, B., Poupeau, J.-J., Tannau, J.-F., Thil, F., Tisnérat-Laborde, N., Valladas, H., 2023. Radiocarbon dating on ECHoMICADAS, LSCE, Gif-sur-Yvette, France: new and updated chemical procedures. Radiocarbon 2023, 1–16.
Hearty, P.J., Neumann, A.C., Kaufman, D.S., 1998. Chevron ridges and runup deposits in the bahamas from storms late in oxygen-isotope substage 5e. Quatern. Res. 50, 309–322.
Heaton, T.J., Köhler, P., Butzin, M., Bard, E., Reimer, R.W., Austin, W.E.N., Bronk Ramsey, C., Grootes, P.M., Hughen, K.A., Kromer, B., Reimer, P.J., Adkins, J., Burke, A., Cook, M.S., Olsen, J., Skinner, L.C., 2020. Marine20 - the marine radiocarbon age calibration curve (0–55,000 cal BP). Radiocarbon 62 (4), 779–820.
Heaton, T.J., Bard, E., Bronk Ramsey, C., Butzin, M., Hatté, C., Hughen, K.A., Köhler, P., Reimer, P.J., 2022. A response to community questions on the Marine20 radiocarbon age calibration curve: marine reservoir ages and the calibration of ^{14}C samples from the oceans. Radiocarbon 65 (1), 247–273.
Hut, G., 1987. Stable isotope reference samples for geochemical and hydrological investigations. In: Consultant Group Meeting IAEA, Vienna, 16–18 September 1985, Report to the Director General. International Atomic Energy Agency, Vienna, p. 42.
Ishizawa, T., Goto, K., Yokoyama, Y., Goff, J., 2020. Dating tsunami deposits: present knowledge and challenges. Earth-Science Reviews 102971.
Kaabouben, F., Baptista, M.A., Ibem Brahim, A., El Mouraouah, A., Toto, A., 2009. On the Moroccan tsunami catalogue. Natural Hazards and Earth Systems Science 9, 1227–1236.
Kelsey, H.M., Witter, R.C., 2020. Radiocarbon dating of tsunami and storm deposits. In: Engel, M., Pilarczyk, J., May, S.M., Brill, D., Garrett, E. (Eds.), Geological Records of Tsunamis and Other Extreme Waves. Elsevier, pp. 663–685.
Ketcham, R.A., 2005. Three-dimensional grain fabric measurements using high-resolution X-ray computed tomography. Journal of Structural Geolology 27, 1217–1228.
Kim, S.T., O'Neil, J.R., 1997. Equilibrium and nonequilibrium oxygen isotope effects in synthetic carbonates. Geochim. Cosmochim. Acta 61 (16), 3461–3475.
Kim, S.T., O'Neil, J.R., Hillaire-Marcel, C., et al., 2007. Oxygen iso- tope fractionation between synthetic aragonite and water: influence of temperature and Mg2+ concentration. Geochimica et Cosmochimica Acta 71 (19), 4704–4715.
Maréchal, C., Boutier, A., Mélières, M.A., Clauzel, T., Betancort, J.F., Lomoschitz, A., Meco, J., Fourel, F., Barral, A., Amiot, R., Lécuyer, C., 2020. Last interglacial Sea surface warming during the sea-level highstand in the Canary Islands: implications for the Canary current and the upwelling off African coast. Quat. Sci. Rev. 234, 106246.
Martins, J.M.M., Martín, A.M., Portela, P.J.C., Soares, A.M.M., 2012. Improving the ^{14}C dating of marine shells from the Canary Islands for constructing more reliable and accurate chronologies. Radiocarbon 54 (3–4), 943–952.
Maxwell, T.A., Haynes, C.V., 1989. Large-scale, low-amplitude bedforms (chevrons) in the Selima Sand Sheet, Egypt. Science 243, 1179–1182.
Meco, J., Petit-Maire, N., Fontugne, M., Shimmield, G., Ramos, A.J., 1997. The Quaternary deposits in lanzarote and fuerteventura (Eastern Canary Islands, Spain): An overview. In: Meco, J., Petit-Maire, N. (Eds.), Climates of the Past: Fuerteventura and Lanzarote. International Union of Geological Sciences, UNESCO, Las Palmas de Gran Canaria, pp. 123–136.
Meco, J., Lomoschitz, A., Rodríguez, Á., Ramos, A.J., Betancort, J.F., Coca, J., 2018. Mid and late Holocene Sea level variations in the Canary Islands. Palaeogeogr. Palaeoclimatol. Palaeoecol. 507, 214–225.
Menéndez, I., Pérez-Chacón, E., Mangas, J., Tauler, E., Engel Brecht, J., Derbyshire, E., Cana, L., Alonso, I., 2014. Dust deposits on La Graciosa Island (Canary Islands, Spain): texture, mineralogy and a case study of recent dust plume transport. Catena 117, 133–144.
Mitra, S., Paris, R., Bernard, L., Abbal, R., Charrier, P., Falvard, S., Costa, P., Andrade, C., 2024. X-ray tomography applied to tsunami deposits: optimized image processing and quantitative analysis of particle size, shape, and sedimentary fabric in 3D. Mar. Geol. 470, 107247.
González Viera, F.J., Morín Pérez, P., Acosta Rodríguez, J.E., 1996. La Graciosa. Estudio Histórico y Geográfico. Centro de la Cultura Popular Canaria, La Laguna.
Ndeye, M., 2008. Marine reservoir ages in Northern Senegal and Mauritania coastal waters. Radiocarbon 50, 281–288.
Nichol, S.L., Goff, J., Devoy, R.J., Chagué-Goff, C., Hayward, B., James, I., 2007. Lagoon subsidence and tsunami on the West Coast of New Zealand. Sediment. Geol. 200, 248–262.
Omira, R., Baptista, M.A., Quartau, R., Ramalho, R.S., Kim, J., Ramalho, I., Rodrigues, A., 2022. How hazardous are tsunamis triggered by small-scale mass-wasting events on volcanic islands? New insights from Madeira – NE Atlantic. Earth Planet. Sci. Lett. 578, 117333.
Pardo-Gordó, S., Vidal-Matutano, P., González-Marrero, M.C., Chávez-Álvarez, M.E., 2023. The 14Canarias web application. An interactive radiocarbon database for the Canary Islands. Journal of Open Archaeology Data 11 (4), 1–6.
Paris, R., Wassmer, P., Sartohadi, J., Lavigne, F., Barthomeuf, B., Desgages, É., Grancher, D., Baumert, Ph., Vautier, F., Brunstein, D., Gomez, Ch., 2009. Tsunamis as geomorphic crisis: lessons from the December 26, 2004 tsunami in Lhok Nga, West Banda Aceh (Sumatra, Indonesia). Geomorphology 104, 59–72.
Paris, R., Ramalho, R.S., Madeira, J., Ávila, S., May, S.M., Rixhon, G., Engel, M., Brückner, H., Herzog, M., Schukraft, G., Perez-Torrado, F.J., Rodriguez-Gonzales, A., Carracedo, J.C., Giachetti, T., 2018. Mega-tsunami conglomerates and flank collapses of ocean island volcanoes. Mar. Geol. 395, 168–187.
Peel, M.C., Finlayson, B.L., McMahon, T.A., 2007. Updated world map of the Köppen-Geiger climate classification. Hydrol. Earth Syst. Sci. 11 (5), 1633–1644.
Perez-Torrado, F.J., Carracedo, J.C., Guillou, H., Rodriguez-Gonzalez, A., Fernandez-Turiel, J.L., 2023. Age, duration, and spatial distribution of ocean shields and rejuvenated volcanism: Fuerteventura and Lanzarote, Eastern Canaries. J. Geol. Soc. London 180 (4) jgs2022–112.
Petit-Maire, N., Delibrias, G., Pomel, S., Rosso, J.C., 1986. Paléoclimatologie des canaries orientales (fuerteventura). Comptes Rendus de l'Académie des Sciences Paris 303, 1241–1246.
Reimer, P.J., Reimer, R.W., 2001. A marine reservoir correction database and on-line interface. Radiocarbon 43 (2A), 461–463.
Reimer, R.W., Reimer, P.J., 2017. An online application for ΔR calculation. Radiocarbon 59 (5), 1623–1627.
Reimer, P.J., Baillie, M.G.L., Bard, E., Bayliss, A., Beck, W.J., Blackwell, P.G., Bronk Ramsey, C., Buck, C.E., Burr, G.S., Edwards, R.L., Friedrich, M., Grootes, P.M., Guilderson, T.P., Hajdas, I., Heaton, T.J., Hogg, A.G., Hughen, K.A., Kaiser, K.F., Kromer, B., McCormac, F.G., Manning, S.W., Reimer, R.W., Richards, D.A., Southon, J.R., Talamo, S., Turney, C.S.M., Van der Pflicht, J., Weyhenmeyer, C.E., 2009. Intcal09 and Marine09 radiocarbon age calibration curves, 0–50,000 years cal BP. Radiocarbon 51 (4), 1111–1150.
Rixhon, G., May, S.M., Engel, M., Mechernich, S., Schroeder-Ritzrau, A., Frank, N., Fohlmeister, J., Boulvain, F., Dunai, T., Brückner, H., 2018. Multiple dating approach (^{14}C, $^{230}Th/U$ and ^{36}Cl) of tsunami-transported reef-top boulders on Bonaire (Leeward Antilles) – current achievements and challenges. Mar. Geol. 396, 100–113.
Rognon, P., Coudé-Gaussen, G., 1996. Paleoclimates off Northwest Africa (28°–35°N) about 18,000 yr B.P. Based on continental eolian deposits. Quat. Int. 46, 118–126.
Santana Cordero, A., Monteiro Quintana, M.L., Hernández Calvento, L., Pérez-Chacón Espino, E., García Romero, L., 2016. Long-term human impacts on the coast of La Graciosa, Canary Islands. Land degradation & development 27 (3), 479–489.
Scheffers, A., Kelletat, D., Scheffers, S.R., Abbott, D.H., Bryant, E.A., 2008. Chevrons enigmatic sedimentary coastal features. Z. Geomorphol. 52 (3), 375–402.
Soares, A.M.M., Martins, J.M.M., Luís Cardoso, J., 2011. Marine radiocarbon reservoir effect of coastal waters off Cape Verde Archipelago. Radiocarbon 53 (2), 289–296.
Soulet, G., Maestrati, P., Gofas, S., Bayon, G., Dewilde, F., Labonne, M., Dennielou, B., Ferraton, F., Siani, G., 2023. Marine reservoir ages for coastal West Africa. Geochronology 5 (2), 345–359.
Spratt, R.M., Lisiecki, L.E., 2016. A Late Pleistocene sea level stack. Climate of the Past 12 (4), 1079–1092.
Stuiver, M, Polach, A., 1977. Discussion: Reporting of ^{14}C Data. Radiocarbon 19 (3), 355–363.
Swart, P.K., Burns, S.J., Leder, J.J., 1991. Fractionation of the stable isotopes of oxygen and carbon in carbon dioxide during the reaction of calcite with phosphoric acid as a function of temperature and technique. Chemical Geology: Isotope Geo- science Section 86, 89–96.
Tisnérat-Laborde, N., Thil, F., Synal, H.-A., Cersoy, S., Hatté, C., Gauthier, C., Massault, M., Michelot, J.-L., Noret, A., Siani, G., Tombret, O., Vigne, J.-D., Zazzo, A., 2015. ECHoMICADAS: a new compact AMS system to measuring ^{14}C for Environment, climate and Human Sciences. In: 22nd International Radiocarbon Conference, Dakar, Senegal, 16-20 November 2015. PHYS-O.05.
Vimpere, L., Kindler, P., Castelltort, S., 2019. Chevrons: Origin and relevance for the reconstruction of past wind regimes. Earth Sci. Rev. 193, 317–332.
Wacker, L., Fülöp, R.H., Hajdas, I., Molnár, M., Rethemeyer, J., 2013. A novel approach to process carbonate samples for radiocarbon measurements with helium carrier gas. Nucl. Instrum. Methods Phys. Res., Sect. B 294, 214–217.

Watts, A.B., 1994. Crustal structure, gravity anomalies and flexure of the lithosphere in the vicinity of the Canary islands. Geophys. J. Int. 119, 648–666.
Williamson, D., Jackson, M., Banerjee, S.K., Petit-Maire, N., 2004. The magnetism of a glacial aeolianite sequence from Lanzarote (Canary Islands): coupling between luvic calcisol formation and Saharan dust trapping processes during wet deposition events off northwestern Sahara. Geophys. J. Int. 157, 1090–1104.
Yanes, Y., Yapp, C.J., Ibáñez, M., Alonso, M.R., De-la-Nuez, J., Quesada, M.L., Castillo, C., Delgado, A., 2011. Pleistocene–Holocene environmental change in the Canary archipelago as inferred from the stable isotope composition of land snail shells. Quatern. Res. 75, 658–669.
Zazo, C., Goy, J.L., Hillaire-Marcel, C., Gillot, P.Y., Soler, V., González, J.A., Dabrio, C.J., Ghaleb, B., 2002. Raised marine sequences of Lanzarote and Fuerteventura revisited – a reappraisal of relative sea-level changes and vertical movements in the eastern Canary Islands during the Quaternary. Quaternary Science Reviews 21, 2019–2046.